Supporting information

Electron self-exchange and self-amplified post-translational modification in the hemoglobins from *Synechocystis* sp. PCC 6803 and *Synechococcus* sp. PCC 7002

Matthew R. Preimesberger,† Matthew P. Pond,† Ananya Majumdar,‡ and Juliette T. J. Lecomte*,†

†T. C. Jenkins Department of Biophysics and ‡Biomolecular NMR Center, Johns Hopkins University, Baltimore, MD 21218

1. Materials

Chemical	Source
Argon	Airgas
bovine hemin chloride	Sigma
bovine liver catalase	Sigma
99.9 % D_2O	Sigma
D-(+)-glucose	Sigma
A. niger glucose oxidase	Sigma
^{15}N ammonium chloride	Sigma
sodium dithionite 85% (DT)	Sigma
urea	J.T. Baker
all other chemicals	Sigma

2. Protein expression and purification: WT and H117A *Synechococcus* GlbN, WT *Synechocystis* GlbN

The following is based on the procedures described in [1-4]. Briefly, wild-type (WT) and variant GlbNs were overexpressed in BL21(DE3) *E. coli* cells. The proteins partitioned primarily into the insoluble fraction. Purified inclusion bodies were solubilized in a 50 mM Tris 1 mM EDTA buffer (pH ~8) containing 8 M urea and then loaded onto a G-50 size exclusion column for concurrent apoGlbN refolding and purification. Fractions containing apoGlbN were identified by SDS-PAGE. Holoproteins were generated by coarse titration with hemin chloride dissolved in 0.1 M NaOH. Excess hemin was removed by passage of the GlbN solution over a DEAE anion exchange column after filtering and centrifugation. GlbN elution was achieved with a 0–0.5 M NaCl gradient. Fractions deemed pure by SDS-PAGE were pooled, concentrated by ultrafiltration, and exchanged into water by dialysis. The purified GlbNs were lyophilized and stored at –20 °C for the long term. The preparation method yielded Fe(III)GlbN (oxidized holoprotein, without post-translational modification). Yields were typically 25 mg /L medium.

Protein concentration determination

Protein concentrations were determined optically. ApoGlbN extinction coefficients were obtained from the ExPASY ProtParam server. HoloGlbN extinction coefficients were determined on a per-heme basis using the pyridine hemochromogen method.[4, 5] Values are listed below. The H117A GlbN variants were assumed to have the same extinction coefficient as the WT protein.

Protein	ε (mM^{-1} cm^{-1})	λ (nm)
apoGlbN		
Synechococcus WT	4.47	280
Synechocystis WT	7.36	280
holoGlbN (Fe(III), bishistidine)		
Synechococcus WT GlbN-R	96	411
Synechococcus WT GlbN-A	87	409
Synechocystis WT GlbN-R	100	411

3. NMR spectroscopy (Method)

Band-selective 1D and 2D ^{15}N-^{1}H HSQC spectroscopy

Standard 2D ^{15}N-^{1}H HSQC experiments were adequate to resolve a small number of NMR signals from Fe(III)GlbN-R, Fe(II)GlbN-A, and Fe(III)GlbN-A. To monitor the conversion of GlbN-R to GlbN-A, we used substoichiometric reduction at high pH (9.2) in order to slow down the reaction. However, significant changes in the concentration of Fe(III)GlbN-R/-A still occurred during 2D acquisition (12 min per experiment), in particular at the beginning when accurate data mattered most. This behavior manifested itself by artificially narrowing (Fe(III)GlbN-A, concentration increasing during indirect acquisition) and broadening (Fe(III)GlbN-R, concentration decreasing during indirect acquisition) HSQC cross peaks in the ^{15}N dimension. The evolving concentrations invalidated a simple quantitative relationship between cross peak volume and concentration, and the 2D approach was abandoned. Raising the pH further was not acceptable because of sample viability.

2D ^{15}N-^{1}H ZZ exchange NMR spectroscopy

The concentration of ferric and ferrous GlbNs must remain constant over the course of the ^{15}N ZZ mixing series in order to extract reliable exchange and relaxation parameters. Experiments were initiated after the solutions had reached a stable ratio of Fe(II) and Fe(III)GlbN. The concentrations were estimated by comparing the integrated intensities of corresponding ferrous and ferric NH peaks obtained from fully relaxed (relaxation delay = 5 s) ^{1}H-^{15}N HSQC experiments. Fe(III):Fe(II) ratios were estimated from these data and were in good agreement with the fitted autopeak intensities (Fe(II)GlbN: $I_{22}(0)$, Fe(III)GlbN: $I_{33}(0)$) at $\tau_{mix} = 0$.

4. Kinetics of the GlbN-R $\rightarrow$ GlbN-A conversion in partially reduced samples

The chemical shift of Thr80 HN (Asn80 in *Synechocystis* GlbN) in each form of *Synechococcus* GlbN (Fe(II)GlbN-R/-A and Fe(III)GlbN-R/-A), is shifted far downfield owing to strong hydrogen bonding with the side chain of His83. Since the ^{15}N chemical shift is nearly degenerate in each form, it was assumed that the band-selective pulse excited Thr80 (Asn80) ^{15}N resonances uniformly. Hence, peak areas obtained using the Topspin 2.1 deconvolution routine were used without correction as target input for kinetic modeling. Although the 80 HN signals from Fe(III)GlbN-R and Fe(III)GlbN-A are resolved because of the distinct magnetic susceptibility tensors of these two paramagnetic species, we suspect that the 80 HN signals of Fe(II)GlbN-R and Fe(II)GlbN-A (both diamagnetic) overlap. We cannot generate a sample of pure wild-type Fe(II)GlbN-R and therefore used *Synechococcus* H117A Fe(II)GlbN as a wild-type GlbN-R mimic to confirm the expectation. Figure S4 shows that the two reduced state cross peaks are not resolved from each other.

The following reactions were used to model the substoichiometric conversion of GlbN at pH 9.2:

$$\text{Fe(II)GlbN-R} \rightarrow \text{Fe(II)GlbN-A} \qquad (1)$$

k_{xl} fixed to 0.0023 s^{-1} as obtained from the optical data (*Synechococcus* GlbN)

or k_{xl} fixed to 0.005 s^{-1}, interpolated from the optical data (*Synechocystis* GlbN)

$$\text{Fe(II)GlbN-A} + \text{Fe(III)GlbN-R} \leftrightarrows \text{Fe(III)GlbN-A} + \text{Fe(II)GlbN-R} \qquad (2)$$

ET step, k_{12} and k_{21} allowed to float

These steps accounted for cross-link propagation. *Synechococcus* GlbN data modeling required an additional minor oxidation phase:

$$\text{Fe(II)GlbN-A} + \text{ox} \rightarrow \text{Fe(III)GlbN-A} + \text{red} \qquad (3)$$
$$k_{ox,app} \text{ allowed to float}$$

This last reaction appeared unrelated to the cross-linking reaction because it was also observed with the unreactive H117A variant (Figure S5). It was assumed that it occurred as a result of contamination with an oxidant (dioxygen). An arbitrary ox concentration was used in Equation 3. The oxidation step was unnecessary to describe the self-amplified conversion of *Synechocystis* GlbN-R to GlbN-A.

Although only a lower limit on individual k_{12} and k_{21} values could be determined reliably, their ratio $K_{12} = k_{12}/k_{21}$ was well described by the data. Since electron self-exchange (ESE) was detected between free GlbN monomers and no additional species was observed in solution, it was likely that GlbN encounter complexes (EC) were weakly populated and in fast exchange on the chemical shift timescale. There was no evidence of Fe(III)GlbN dimerization in samples up to 5 mM protein. If one assumes that k_{12} and k_{21} report on ET directly or that association and dissociation steps are fast and symmetrical about encounter complex formation (identical work terms):

$$\text{Fe(II)GlbN-A} + \text{Fe(III)GlbN-R} \leftrightarrows \text{EC} \leftrightarrows \text{EC*} \leftrightarrows \text{Fe(III)GlbN-A} + \text{Fe(II)GlbN-R} \quad (4),$$

then the ratio k_{12}/k_{21} may be interpreted in terms of redox potential using:

$$\Delta E° = -\Delta G°/nF = (RT \ln K_{12})/nF \qquad (5)$$

For *Synechococcus* GlbN, K_{12} was 0.1, returning $\Delta E° \sim -60$ mV (GlbN-R lower potential). For *Synechocystis* GlbN, K_{12} was 0.25, returning $\Delta E° \sim -35$ mV (GlbN-R lower potential). The latter $\Delta E°$ is about 50 mV less than the difference in measured redox potentials between WT *Synechocystis* GlbN-A and H117A *Synechocystis* GlbN (–85 mV, H117A lower) [6]. This suggests either that the observed K_{12} does not report directly on ET and/or that H117A *Synechocystis* GlbN is an imperfect analogue for WT *Synechocystis* GlbN-R redox behavior.

5. Electron self-exchange rate

The exchange of longitudinal $^{15}N_Z$ magnetization as a function of τ_{mix} generates self (I_{22} and I_{33}) and cross (I_{23} and I_{32}) peaks whose integrated intensities are described by the Bloch-McConnell equations [7].

In the GlbN analyses, fitting was reserved for residues that exhibited completely resolved $^{15}N_Z$ exchange quartets and similar ^{1}H line widths in the Fe(II) and Fe(III) states (data for WT *Synechococcus* GlbN-A shown, Figure S10, with probe location in the 2KSC structure shown in Figure S12). The proximal coordinating histidine (His70), though resolved, was removed from the analysis because of its non-negligible paramagnetic relaxation enhancement in the ferric state. No correction was made for differential relaxation during INEPT transfers. Peak volumes

were estimated by Gaussian simulation using the program Sparky. The relevant equations are [8]:

$$I_{22}(\tau) = I_{22}(0)[-(\lambda_2-a_{11})\exp(-\lambda_1\tau) + (\lambda_1-a_{11})\exp(-\lambda_2\tau)]/(\lambda_1-\lambda_2)$$

$$I_{33}(\tau) = I_{33}(0)[-(\lambda_2-a_{22})\exp(-\lambda_1\tau) + (\lambda_1-a_{22})\exp(-\lambda_2\tau)]/(\lambda_1-\lambda_2)$$

$$I_{23}(\tau) = I_{22}(0)[a_{21}\exp(-\lambda_1\tau)-a_{21}\exp(-\lambda_2\tau)]/(\lambda_1-\lambda_2)$$

$$I_{32}(\tau) = I_{33}(0)[a_{12}\exp(-\lambda_1\tau)-a_{12}\exp(-\lambda_2\tau)]/(\lambda_1-\lambda_2)$$

with $\lambda_{1,2} = (1/2)\{(a_{11} + a_{22}) \pm [(a_{11} - a_{22})^2 + 4k_{23}k_{32}]^{1/2}\}$ and $a_{11} = R_{1,2} + k_{23}$, $a_{22} = R_{1,3} + k_{32}$, $a_{12} = -k_{32}$, $a_{21} = -k_{23}$. I_{22} and I_{33} refer to the intensity of the Fe(II) auto peak and Fe(III) auto peak, respectively; I_{23} refers to the intensity of the exchange cross peak with Fe(II) ^{15}N and Fe(III) ^{1}H shifts; I_{32} refers to the intensity of the exchange cross peak with Fe(III) ^{15}N and Fe(II) ^{1}H shifts; k_{23} refers to the apparent first order rate constant for Fe(II) $\rightarrow$ Fe(III), and k_{32} refers to the apparent first order rate constant for Fe(III) $\rightarrow$ Fe(II).

The data (truncated to $\tau_{mix} < 500$ ms) were first inspected by calculating the $\Xi(t)$ ratio, which is unaffected by relaxation [9].

$$\Xi(t) = \frac{I_{23}(t)I_{32}(t)}{I_{22}(t)I_{33}(t) - I_{23}(t)I_{32}(t)} = k_{32}k_{23}t^2$$

Global fitting (Scilab 5.2, not shown) indicated that all chosen residues (and presumably the whole protein) registered a single exchange process. A local nonlinear least squares fitting routine (Scilab 5.2) was also employed to extract preliminary guesses for exchange (k_{23}, k_{32}), relaxation ($R_{1,2}$, $R_{1,3}$), and intensity ($I_{22}(0)$, $I_{33}(0)$) parameters by minimization of the sum of the squared error residuals.

Uncertainties in peak volumes were re-estimated by calculating the standard deviation of the residuals between best-fit curves and data. Uncertainties estimated in this fashion were of similar magnitude as those estimated from the analysis of duplicate τ_{mix} points. The program KinTek Explorer was used to extract the reported exchange and relaxation parameters by simulation and nonlinear least squares fitting of integrated peak intensity data directly to the kinetic scheme:

$$\text{Fe(II)N}_z\text{(eq)} \leftarrow \text{Fe(II)N}_z(\tau_{mix}) \leftrightarrows \text{Fe(III)N}_z(\tau_{mix}) \rightarrow \text{Fe(III)N}_z\text{(eq)}$$

Owing to a small uncertainty in the relative concentration of Fe(II) and Fe(III) GlbNs, $I_{22}(0)$ and $I_{33}(0)$ were allowed to float independently in this analysis. The relative intensity of initial Fe(II) and Fe(III) GlbN magnetization ($I_{22}(0)/I_{33}(0)$) converged to values that were in good agreement with those determined by analysis of fully-relaxed HSQC data. Extracted ^{15}N R_1 values were generally within error of those determined by conventional methods (these are shown in Figure S10 for *Synechococcus* WT GlbN-A and illustrate the influence of the paramagnetic center). Residue-specific exchange parameters were within error of one another and further confirmed that a single exchange event was sufficient to characterize the ET reaction between free Fe(II) and Fe(III) GlbN monomers in solution.

KinTek Explorer confidence contours were calculated on a per-residue basis (one example is shown in Figure S13). Individual best-fit parameters were allowed to vary at least 20-fold when computing confidence contours. A threshold $\chi^2_{limits}/\chi^2_{min}$ value of 1.5 was used to evaluate the confidence contour error bounds. The 1.5-fold χ^2_{min} acceptable error boundary was chosen based on the following information: number of data points = 44–48, number of fitted parameters = 6 (k_{23}, k_{32}, $R_{1,2}$, $R_{,3}$ and $I_{22}(0)$, $I_{33}(0)$ scaling factors), and degrees of freedom = 38–42.

This method of analysis was applied to H117A *Synechococcus* GlbN (4 resolved ZZ quartets) and WT *Synechocystis* GlbN-A (3 resolved ZZ quartets). Figure S14 shows the fitted data used to provide k_{22} in the text for H117A *Synechococcus* GlbN, and Figure S15 presents an example N_z evolution curve used to estimate the kinetics of ESE in WT *Synechocystis* GlbN-A.

6. Structural calculations

The magnetic susceptibility tensor obtained by refinement had moderate anisotropy: $\Delta\chi_{ax} = (3.94 \pm 0.07) \times 10^{-32}$ m^3 and $\Delta\chi_{rh} = (1.07 \pm 0.06) \times 10^{-32}$ m^3. The Euler angles were $\alpha = 257°$, $\beta = -16°$, $\gamma = 27°$. (Note that Numbat [10] uses the "ZYZ" convention for Euler rotation.) The molecular frame of reference had x axis along the Fe–NC direction and z axis pointing toward the proximal histidine; the coordinates of the Fe center were fixed at the origin. Tensor representations in Figures S19–S21 were prepared with Numbat [10]. Additional spectral assignments will be necessary to improve the tensor calculation.

REFERENCES

1. Scott NL, Lecomte JTJ (2000) Protein Sci. 9:587-597
2. Scott NL, Falzone CJ, Vuletich DA, Zhao J, Bryant DA, Lecomte JTJ (2002) Biochemistry 41:6902-6910
3. Vuletich DA, Falzone CJ, Lecomte JTJ (2006) Biochemistry 45:14075-14084
4. Nothnagel HJ, Preimesberger MR, Pond MP, Winer BY, Adney EM, Lecomte JTJ (2011) J. Biol. Inorg. Chem. 16:539-552
5. de Duve C (1948) Acta Chem. Scan. 2:264-289
6. Hoy JA, Smagghe BJ, Halder P, Hargrove MS (2007) Protein Sci. 16:250-260
7. John M, Headlam MJ, Dixon NE, Otting G (2007) J. Biomol. NMR 37:43-51
8. Farrow NA, Zhang O, Forman-Kay JD, Kay LE (1995) Biochemistry 34:868-878
9. Miloushev VZ, Bahna F, Ciatto C, Ahlsen G, Honig B, Shapiro L, Palmer AG, 3rd (2008) Structure 16:1195-1205
10. Schmitz C, Stanton-Cook MJ, Su XC, Otting G, Huber T (2008) J. Biomol. NMR 41:179-189

Electron self-exchange rate in wild-type *Synechococcus* GlbN-A. Values were determined at 298 K and pH 9.2. The second order rate constant for ESE was obtained by summing k_{23} and k_{32} and dividing by the total concentration of protein (~2 mM). Subscripts 2 and 3 stand for Fe(II) and Fe(III), respectively.

Residue (local)		$R_{1,2}$	$R_{1,3}$	k_{23} (s^{-1})	k_{32} (s^{-1})
Leu91, best fit		1.66	1.67	0.52	0.42
	lower bound	1.56	1.58	0.41	0.33
	upper bound	1.80	1.75	0.62	0.50
Leu122, best fit		1.56	1.64	0.61	0.36
	lower bound	1.39	1.58	0.48	0.34
	upper bound	1.71	1.70	0.71	0.39
Gln71, best fit		1.72	1.65	0.42	0.39
	lower bound	1.64	1.60	0.38	0.36
	upper bound	1.79	1.69	0.47	0.42
Phe35, best fit		1.61	1.72	0.50	0.34
	lower bound	1.50	1.64	0.44	0.27
	upper bound	1.72	1.81	0.57	0.40
Arg124, best fit		1.57	1.62	0.56	0.44
	lower bound	1.41	1.51	0.47	0.39
	upper bound	1.73	1.73	0.65	0.48

Electron self-exchange rate in H117A *Synechococcus* GlbN. Values determined at 298 K and pH 9.2. The total concentration of protein was ~1.7 mM, which was used to calculate the second order rate constant for ESE as described above. Subscripts 2 and 3 stand for Fe(II) and Fe(III), respectively.

Residue (local)		$R_{1,2}$	$R_{1,3}$	k_{23} (s^{-1})	k_{32} (s^{-1})
Gln47, best fit		1.72	1.67	0.45	0.17
	lower bound	1.61	1.58	0.41	0.15
	upper bound	1.84	1.75	0.48	0.19
Peak X, best fit		1.64	1.63	0.44	0.14
	lower bound	1.53	1.55	0.38	0.13
	upper bound	1.77	1.70	0.50	0.16
Gln71, best fit		1.68	1.66	0.40	0.16
	lower bound	1.57	1.55	0.34	0.15
	upper bound	1.81	1.78	0.45	0.17
Arg124, best fit		1.52	1.61	0.58	0.17
	lower bound	1.41	1.53	0.49	0.15
	upper bound	1.63	1.68	0.67	0.20

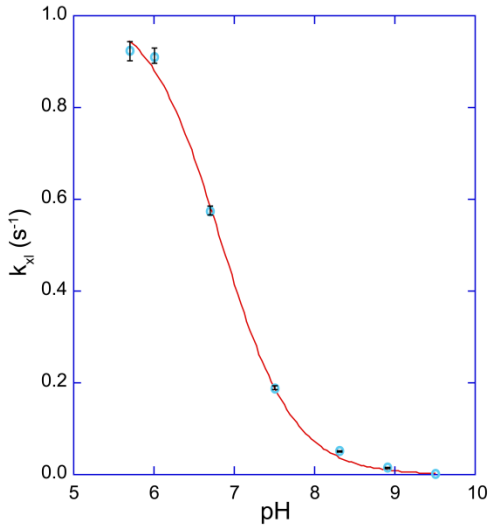

Figure S1: pH dependence of the cross-linking rate constant for *Synechocystis* WT GlbN. The k_{xl} value was determined in triplicate at each pH. The solid line represents a fit with pK_a = 6.83 ± 0.06 and Hill coefficient n = 0.96 ± 0.09 (Equation 1 in the text). The maximum rate constant was estimated as $k_{xl,max}$ = 1.02 ± 0.04 s^{-1}. Because of the lack of an acid baseline, the pK_a value is tentative. Error bars were generated by taking the maximal upper and lower bounds of k_{xl} derived from KinTek Explorer confidence contour analysis using a threshold $\chi^2_{limits}/\chi^2_{min}$ value of 1.2. The pH 9.5 k_{xl} value has been previously determined by manual mixing methods [4], and was included in this analysis.

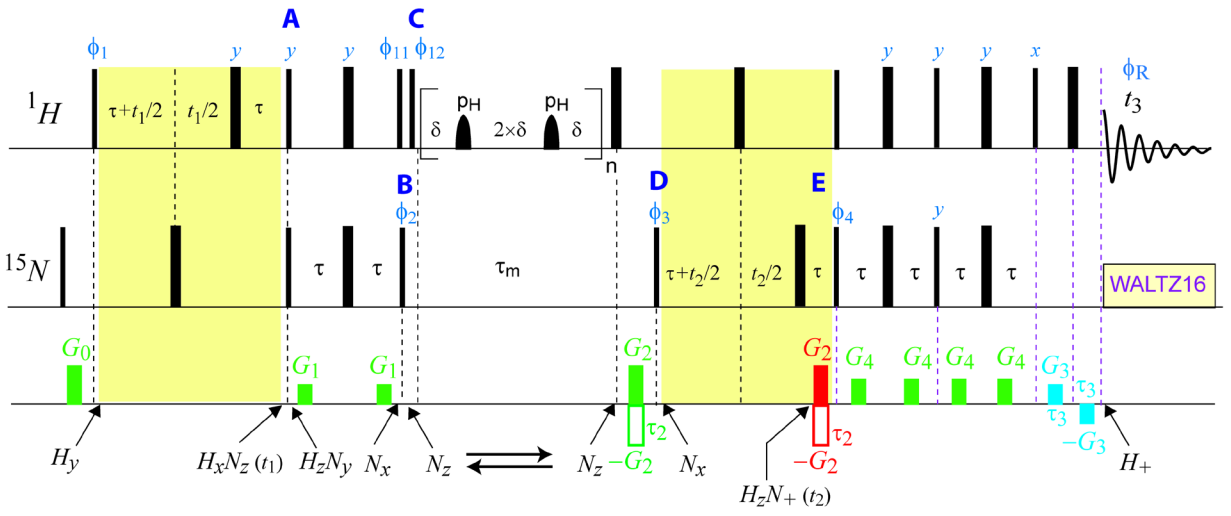

Figure S2: Pulse sequence for the SE H–Nz-N–H ZZ exchange experiment. Narrow and wide black bars denote 90° and 180° pulses, respectively. $\phi_1 = x, -x$ + States/TPPI; $\phi_{11} = y$ + States/TPPI; $\phi_{12} = -x, x$; $\phi_2 = 2(y),2(-y)$; $\phi_3 = 4(y),4(-y)$ + States/TPPI; $\phi_4 = x$ + echo/antiecho; $\phi_R = x, -x, -x, x, -x, x, x, -x$. The minimum number of scans is 4. At point A, ^{1}H magnetization has been frequency labeled (t_1 max = 25 ms) with INEPT transfer achieved by setting τ to $1/(4J_{NH})$ = 2.3 ms. Anti-phase H_zN_y magnetization evolves to in-phase $^{15}N_x$ during the second INEPT period and is placed along the z-axis after the ^{15}N pulse at point B. Quadrature detection of $^1H(\omega_1)$ is achieved through States-TPPI cycling. Additional phase cycling of the initial ^{1}H 90° and the ^{1}H 90° at point C is required to place H_2O magnetization at equilibrium during the mixing period. The ZZ mixing time in Figure 5 was 484 ms (approximate optimal τ_{mix} for cross-peak buildup during the *Synechococcus* WT GlbN-A ESE reaction). Similar to the 2D ^{15}N ZZ experiments, an even number of equally spaced 180° G^3 ^{1}H selective 1.0-ms pulses is applied 3.3 kHz downfield of the carrier (4.76 ppm) to eliminate heteronuclear cross-correlated relaxation and minimize water saturation during τ_{mix} ($\tau_{mix} = n \times (4\delta + 2\ p_H)$, δ = 5 ms, $p_H \sim H^N$ selective 180° pulse). After the mixing period, $^{15}N_z$ magnetization is rotated into the transverse plane (point D) for chemical shift evolution (maximum t_2 = 49.4 ms). Gradient-encoded H_ZN_+ magnetization is generated at point E. ^{15}N (ω_2) quadrature detection is achieved using echo-antiecho coherence selection. A sensitivity-enhanced reverse INEPT element was utilized to prepare ^{1}H magnetization for direct detection (τ_2 = 1 ms; τ_3 = 0.1 ms; $G_3 \sim 0.5 \times G_2$). WALTZ16 ^{15}N decoupling was performed during FID acquisition (t_3 = 60 ms). The relaxation delay was set to 0.9 s and the total acquisition time was approximately 60 h.

One advantage of this exchange experiment compared to collecting spectra of the pure reduced (Figure S16) and oxidized forms individually is that the chemical shifts of each species are obtained under identical conditions of ionic strength, pH and temperature.

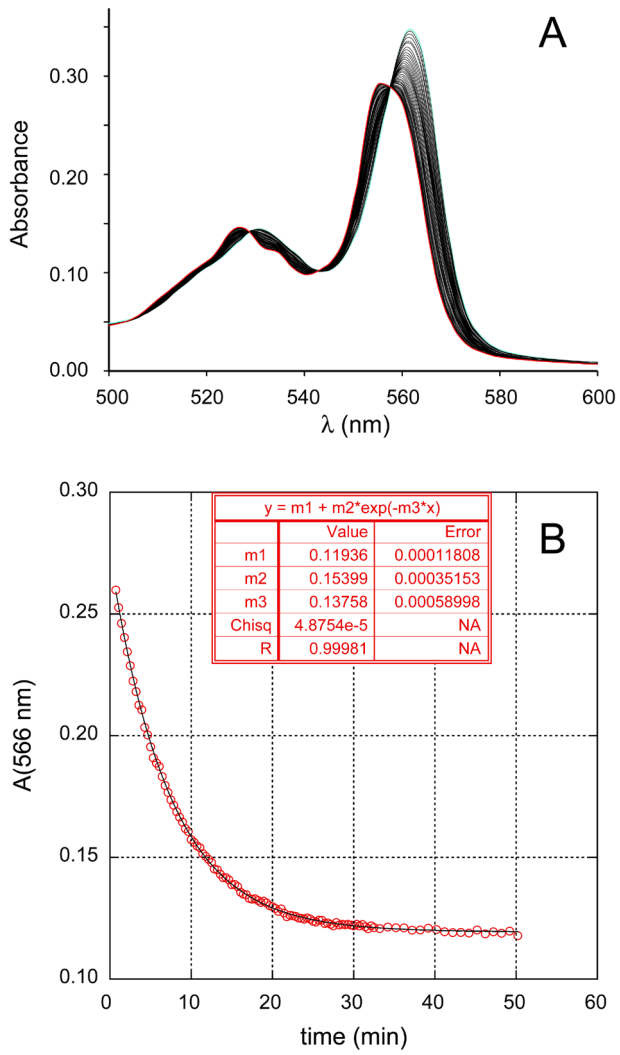

Figure S3: Conversion of *Synechococcus* WT GlbN-R to GlbN-A following reduction with excess DT at pH 9.2 monitored by optical absorbance. (A) The first spectrum is shown in cyan; the spectrum collected after 1 h is in red. Isosbestic points were detected for the first 30 to 45 min. After this period of time, spectral deterioration resembling that when treating the protein with H_2O_2 was observed. This was attributed to the release of peroxide following deactivation of catalase in the dioxygen scavenging system in the presence of excess DT. The data were collected over 20 h and processed by SVD in order to extract the rate constant for the conversion step. (B) Time course of the absorbance at 566 nm. The value of k_{xl} was $(2.3 \pm 0.1) \times 10^{-3}$ s^{-1}.

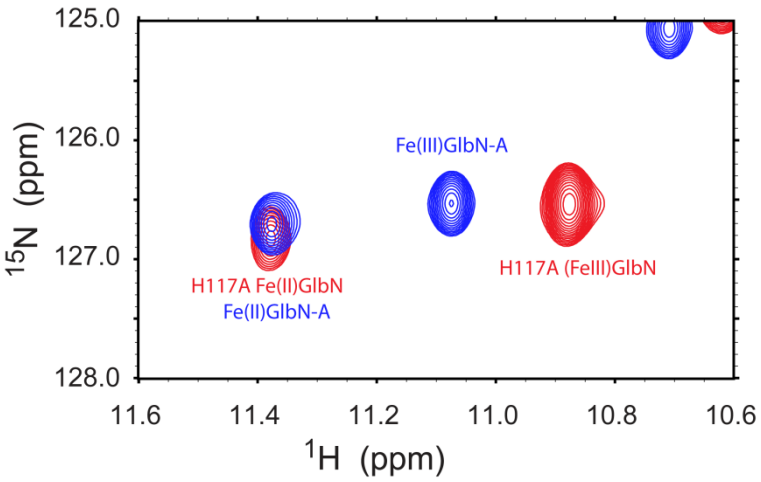

Figure S4: Overlay of two ^{1}H-^{15}N HSQC spectra of *Synechococcus* GlbN. The region contains signals from Thr80 HN. The two samples were mixtures of WT Fe(II) and Fe(III) GlbN-A (blue) and H117A Fe(II) and Fe(III) GlbN (red). The figure illustrates the overlap of the H117A Fe(II)GlbN and Fe(II)GlbN-A signals, which leads us to assume that the signals of WT Fe(II)GlbN-R and Fe(II)GlbN-A also overlap. Trace "a" in Figure 4a in the main text therefore contains intensity from both species. The *Synechocystis* GlbN conversion data were modeled assuming a similar overlap between the Asn80 HN signals in Fe(II)GlbN-R and Fe(II)GlbN-A (trace "d" in Figure 4b).

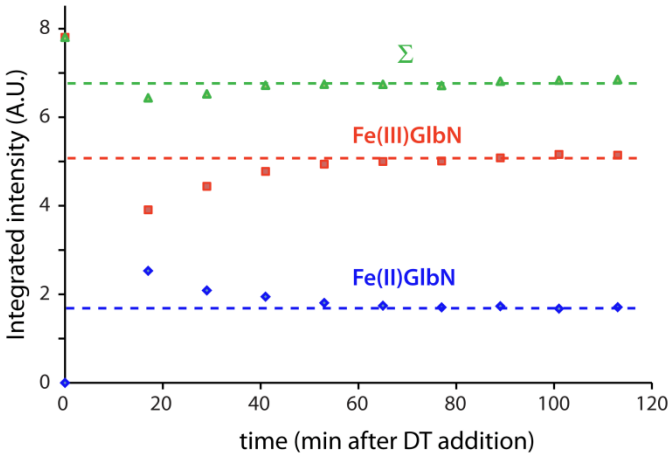

Figure S5: Time course of Thr80 HN signals for *Synechococcus* H117A Fe(II)GlbN (blue) and Fe(III)GlbN (red) after substoichiometric reduction in the presence of GODCAT. Integrated intensities were estimated by Gaussian simulation of cross peaks in 2-D ^{1}H-^{15}N HSQC data. The decrease in the intensity of the Fe(II) form is compensated by an increase in the intensity of the Fe(III) form. This is attributed to partial reoxidation of the sample, likely by dioxygen as a contaminant.

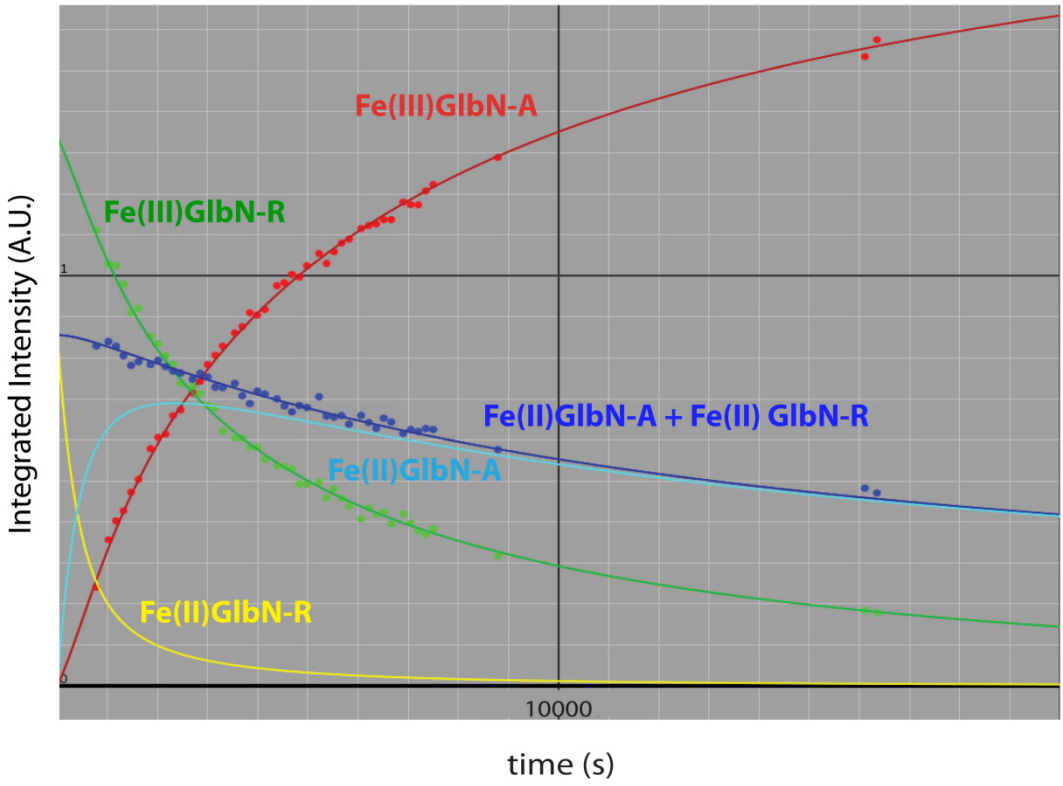

Figure S6: Time course of *Synechococcus* Fe(II)GlbN-R, Fe(III)GlbN-R, Fe(II)GlbN-A, and Fe(III)GlbN-A after substoichiometric reduction in the presence of GODCAT. The decrease in the intensity of the total Fe(II) protein is compensated by an increase in the intensity of the total Fe(III) protein. The data were simulated using the program KinTek Explorer and the lines represent a nonlinear least-squares fit of the data to the ET model (Equations 1, 2, and 3 in text above). The uncertainty of fitted parameters is discussed in the text and in Figure S7.

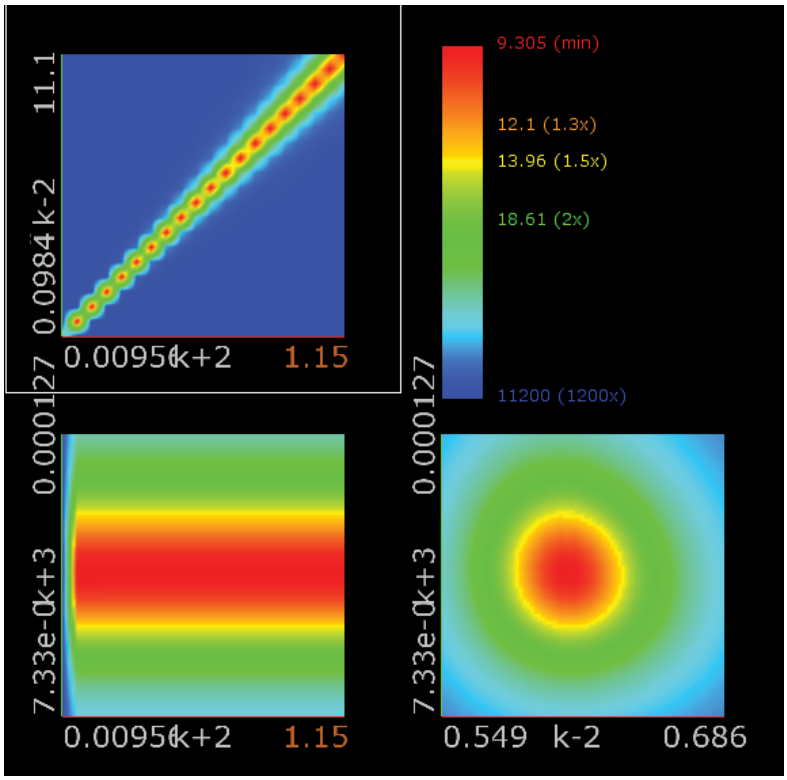

Figure S7: Confidence contour for the fit in Figure S6. Here, k_{+2} is the same as k_{12} in the text and k_{-2} corresponds to k_{21}; k_{+3} is the bimolecular rate constant for reoxidation. χ^2 Contours in yellow correspond to a $\chi^2_{limits}/\chi^2_{min} = 1.5$. This plot shows that the ratio of k_{12} and k_{21} (and not individual values) is well defined by the data.

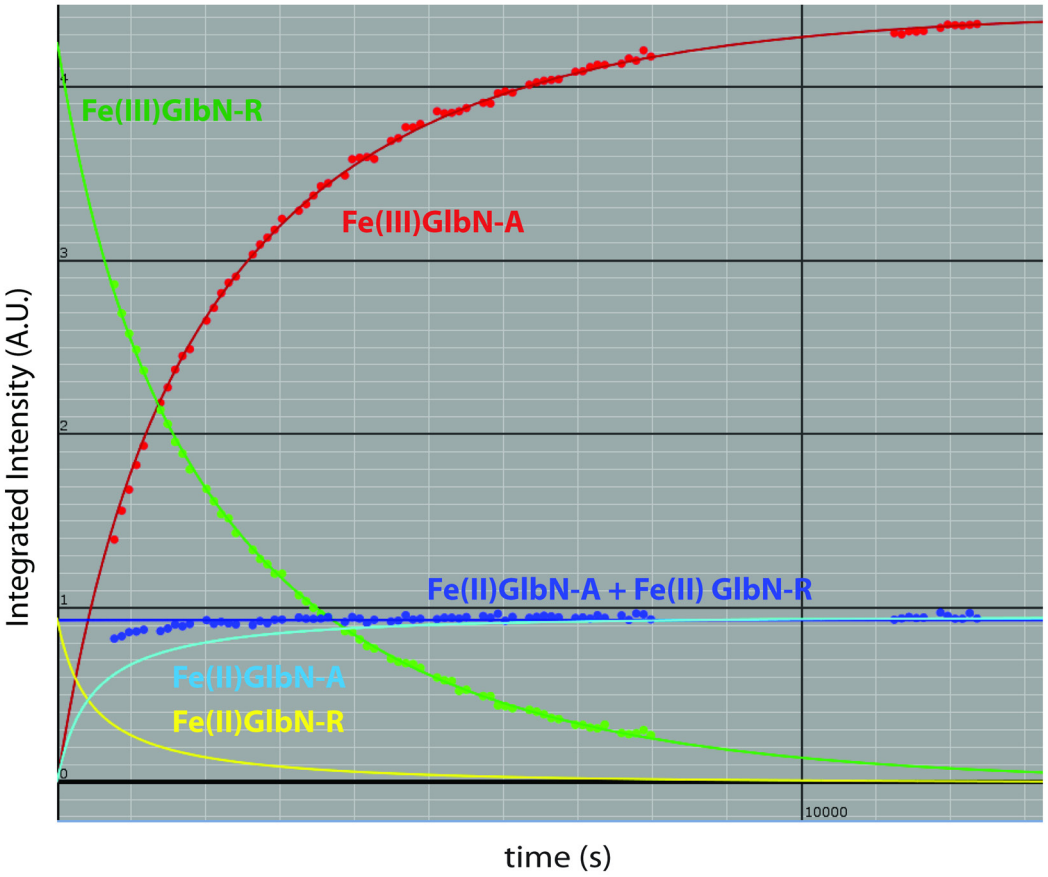

Figure S8: Time course of *Synechocystis* Fe(II)GlbN-R, Fe(III)GlbN-R, Fe(II)GlbN-A, and Fe(III)GlbN-A after substoichiometric reduction in the presence of GODCAT. The decrease in the intensity of the total ferrous protein is compensated by an increase in the intensity of the total ferric protein and the kinetics are consistent with a single ET step. *Synechocystis* Fe(II)GlbN remained at a constant concentration throughout the self-amplified conversion reaction. The data were simulated using the program KinTek Explorer and the lines represent a nonlinear least squares fit of the data directly to the ET model (Supplemental equations 1 and 2).

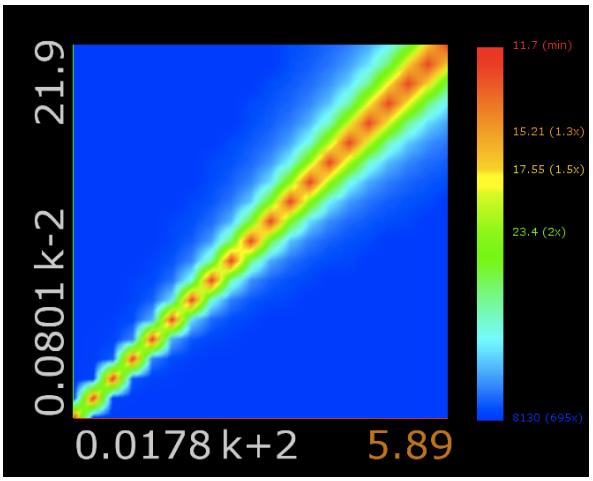

Figure S9: Confidence contour for the fit in Figure S8. Here, k_{+2} (in text, k_{12})corresponds to the *Synechocystis* WT Fe(II)GlbN-A to Fe(III)GlbN-R cross-exchange rate constant, and k_{-2} (in text, k_{21}) corresponds to the reverse reaction, in which Fe(II)GlbN-R transfers an electron back to Fe(III)GlbN-A. χ^2 Contours in yellow correspond to a $\chi^2_{limits}/\chi^2_{min} = 1.5$. The NMR data define the ratio of k_{12} and k_{21} but only provide a lower bound on $k_{12} \sim 10\ M^{-1}\ s^{-1}$. The apparent equilibrium constant observed for *Synechocystis* WT GlbN was $K_{12} = k_{12}/k_{21} = 0.25$.

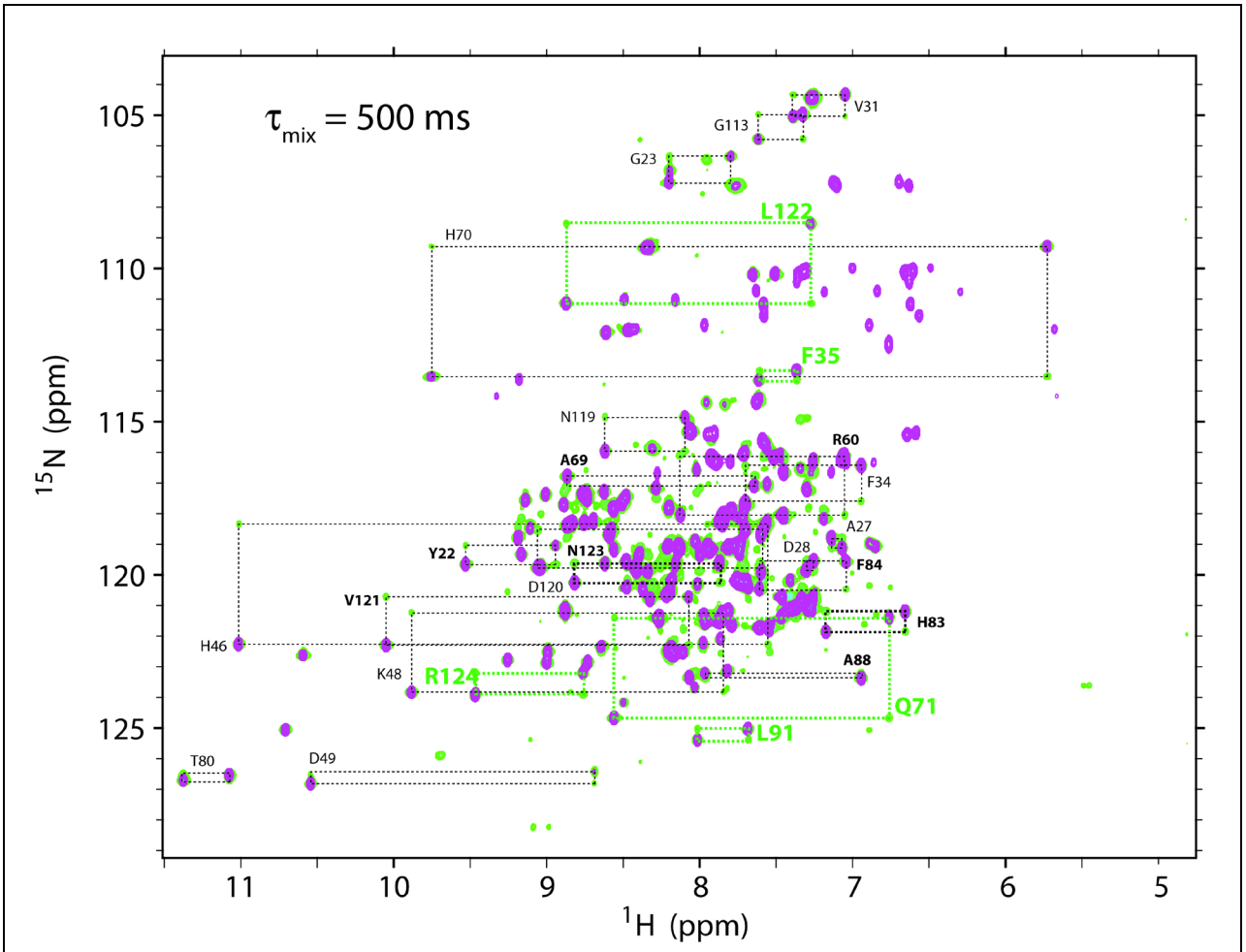

Figure S10: An ^{15}N ZZ exchange spectrum (green) overlaid onto a standard ^{1}H-^{15}N HSQC spectrum (magenta) collected on a 40:60 Fe(II):Fe(III) redox mixture of *Synechococcus* WT GlbN-A (inset of Figure 5 in the main text) showing the resolved exchange quartets chosen for ESE rate determination (annotated in green).

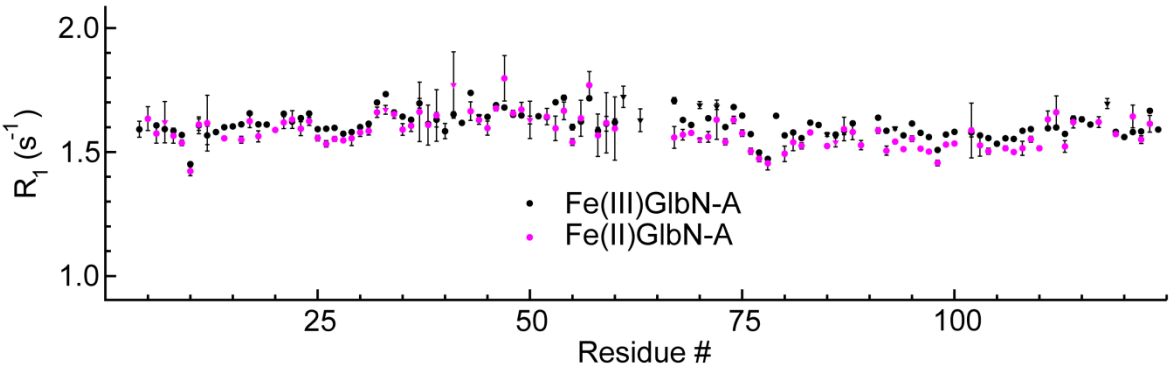

Figure S11: ^{15}N R_1 versus residue number for *Synechococcus* WT Fe(III)GlbN-A and Fe(II)GlbN-A. Note that the values for the reduced state are systematically lower than those of the oxidized state, but by a small percentage that in most cases is within experimental error. The values were consistent with those obtained in the fitting of the ^{15}N ZZ exchange experiments.

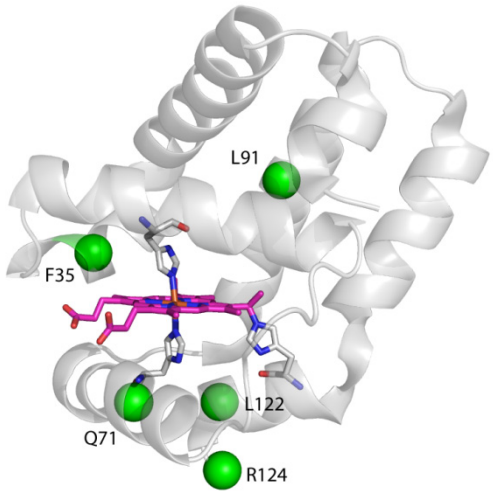

Figure S12: The five probes used in the analysis of the *Synechococcus* WT GlbN-A ^{15}N ZZ exchange data are shown as green spheres on the solution structure of *Synechococcus* WT GlbN-A (2KSC). As expected, the probes all report on the same exchange event corresponding to ESE.

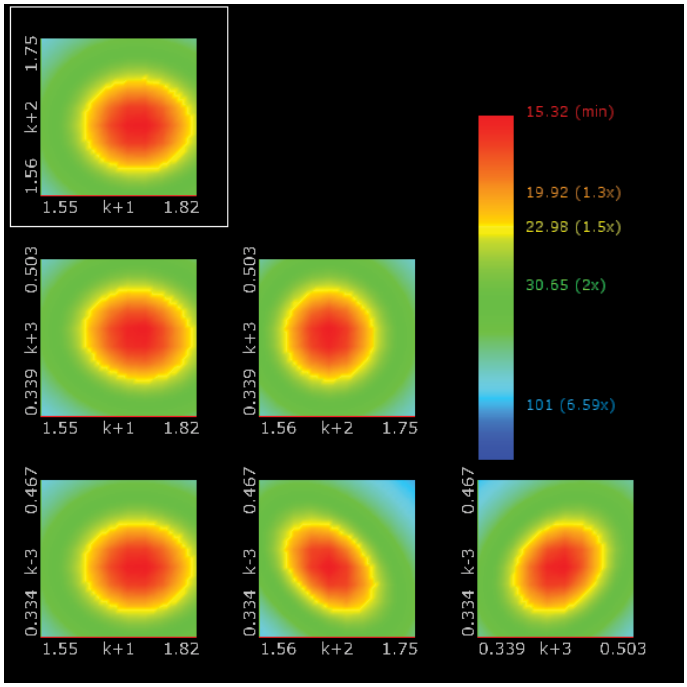

Figure S13: Confidence contour for the fit shown in Figure 5 of the main text (Gln71). Here, k_{+1} and k_{+2} are the ^{15}N R_1 values in *Synechococcus* WT Fe(II) and Fe(III) GlbN-A respectively. k_{+3} and k_{-3} are the apparent 1st order rate constants that characterize N_z magnetization exchange during τ_{mix} due to ESE. k_{+3} (k_{-3}) reports on indirectly detected ferrous (ferric) magnetization that was subsequently transferred to ferric (ferrous) GlbN-A for direct detection. The yellow regions of the χ^2 contour plots correspond to a $\chi^2_{limits}/\chi^2_{min} = 1.5$.

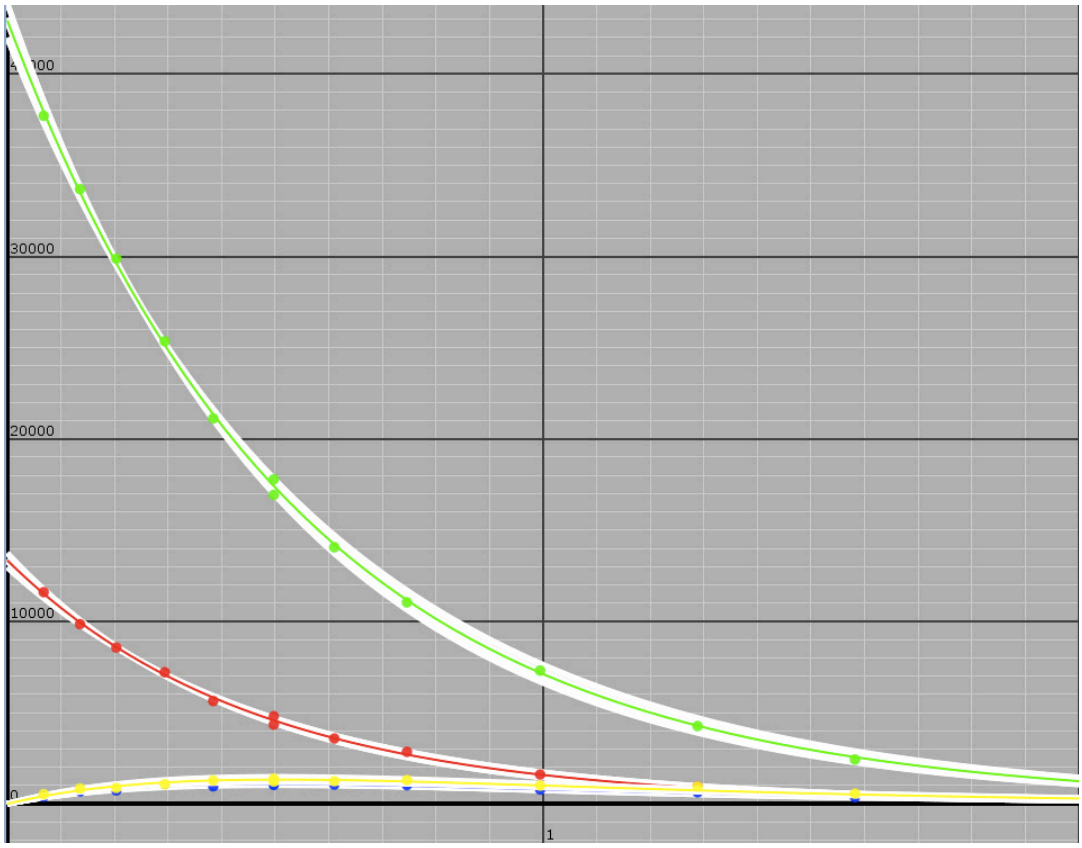

Figure S14: Sample fit for Nz ZZ exchange detected ESE in *Synechococcus* H117A GlbN (Q47 HN). The white regions define the lower and upper bounds determined from KinTek Explorer confidence contour analysis ($\chi^2_{limits}/\chi^2_{min} = 1.5$).

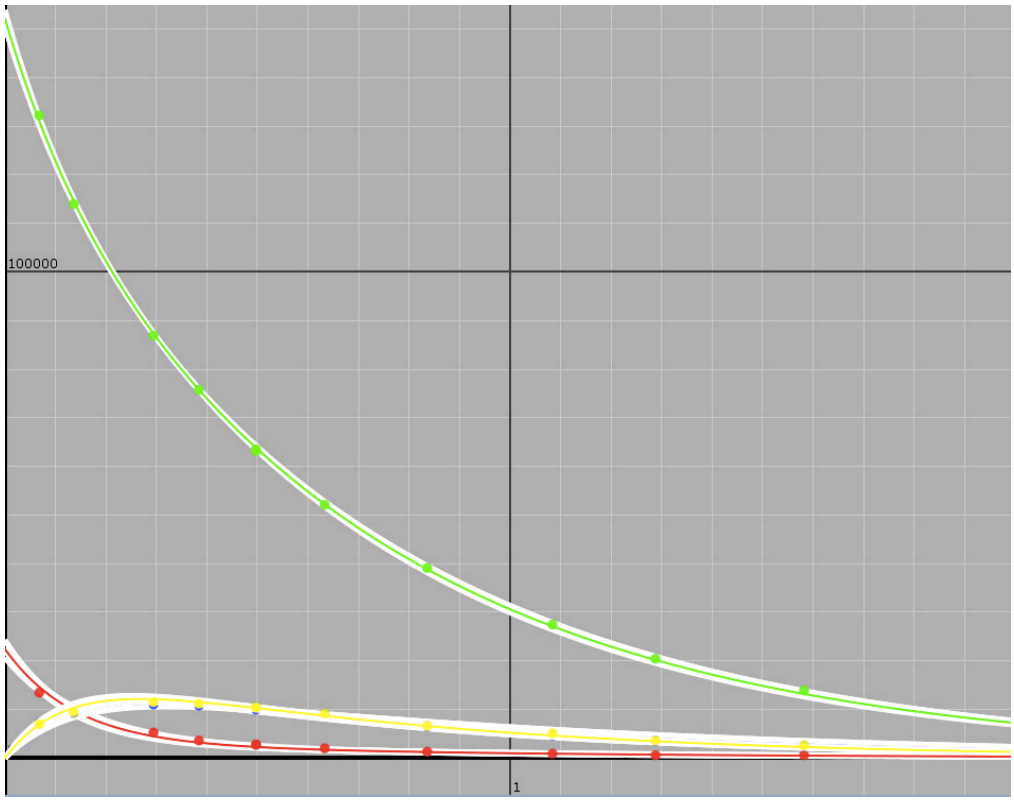

Figure S15: Sample fit to determine the ESE kinetics of *Synechocystis* WT GlbN-A using Nz ZZ exchange NMR. The Fe(II) GlbN-A ^{15}N R_1 uncertainty is relatively large owing to low auto-peak intensities. The ESE rate constants were determined with reasonable accuracy; the white traces describe the upper and lower error bounds for $\chi^2_{limits}/\chi^2_{min} = 1.5$.

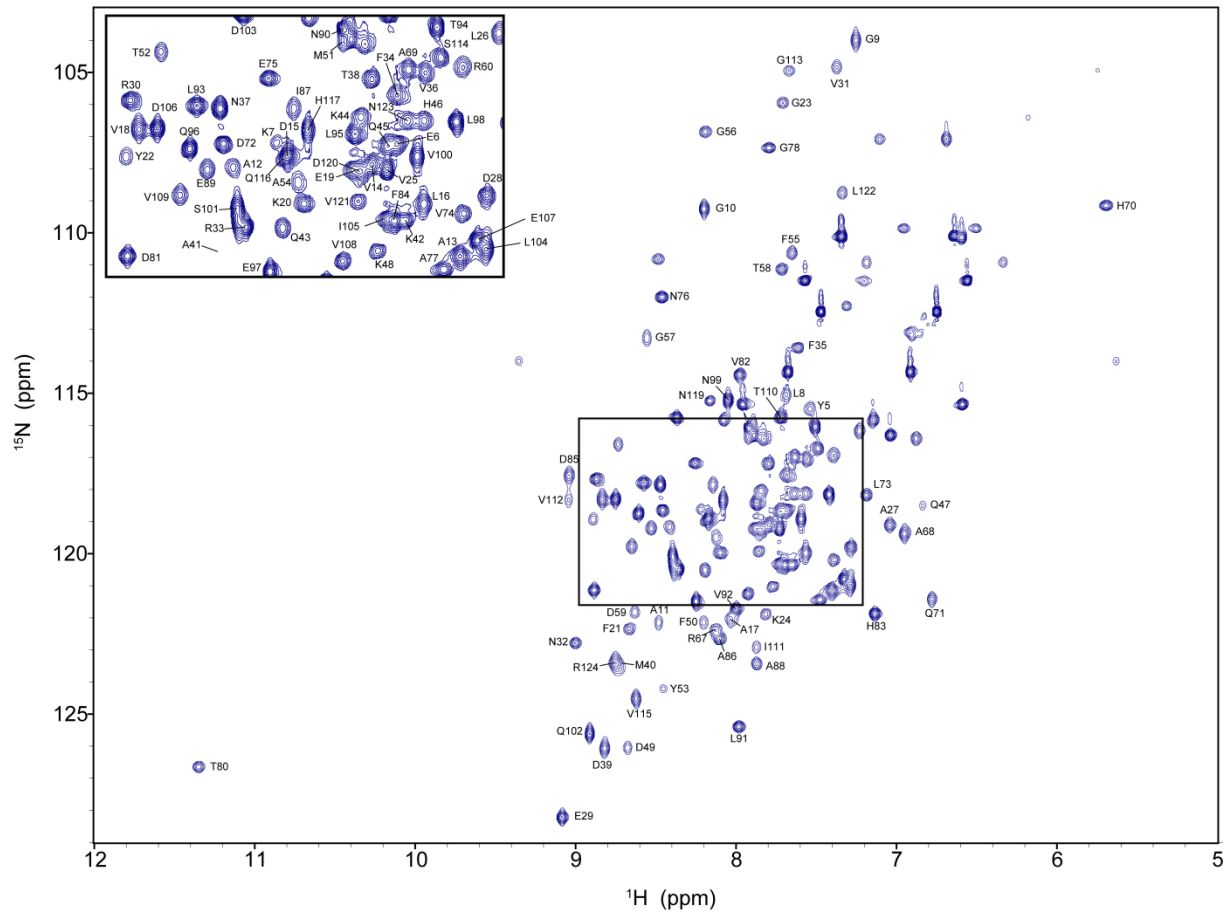

Figure S16: An assigned ^{1}H-^{15}N HSQC spectrum of *Synechococcus* WT Fe(II)GlbN-A (600 MHz, 298 K, 100 mM phosphate buffer, pH 7.2, 10% D_2O). The sample contained ~1.6 mM GlbN and GODCAT. Note that the line widths are variable. For example, broader cross peaks are observed at the end of the E helix (residues 47–54). Backbone ^{1}H chemical shifts of Fe(II)GlbN-A used in the TALOS+ and pseudocontact shift calculations have been deposited at the BMRB (accession number 17947).

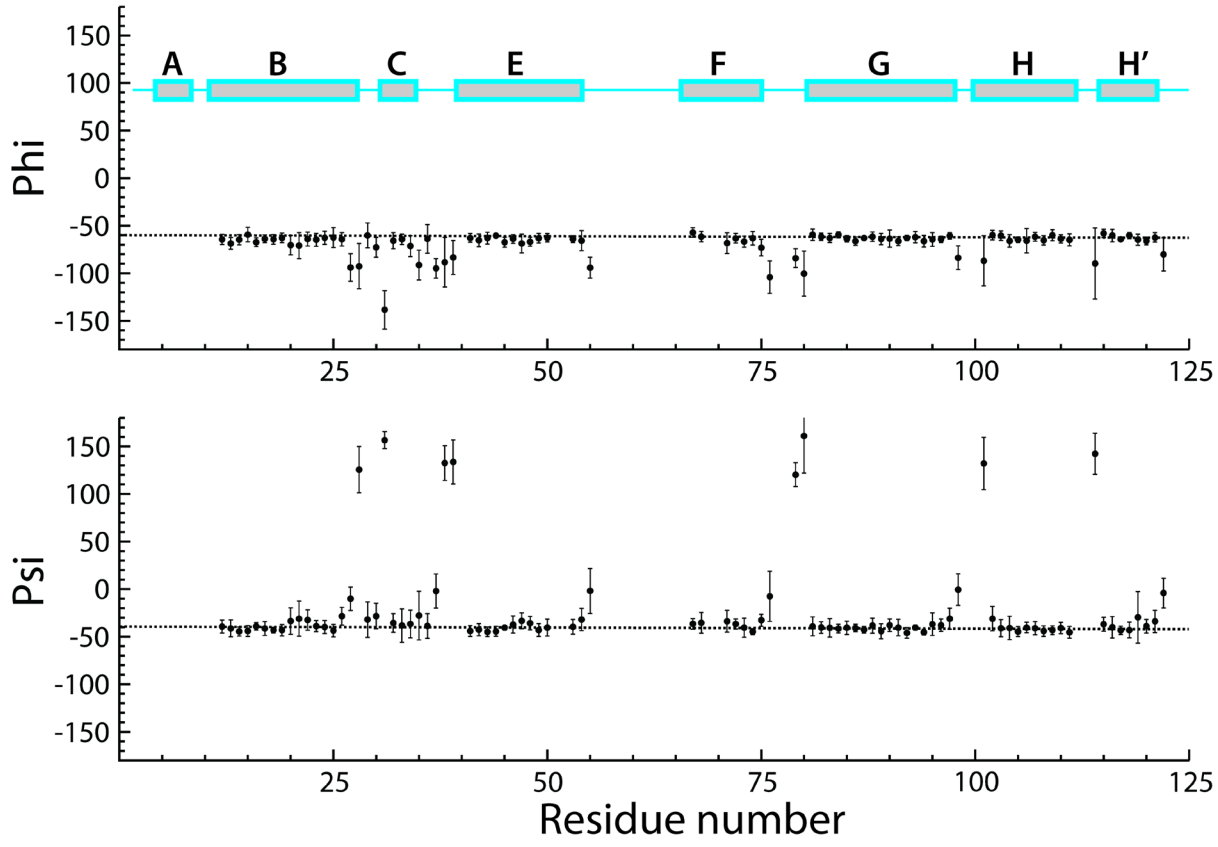

Figure S17: Backbone dihedral angles and their uncertainties for *Synechococcus* WT Fe(II)GlbN-A calculated with TALOS+. The secondary structure observed in Fe(III)GlbN-A, indicated by rectangles, is maintained. Dotted lines are drawn at $\varphi = -60°$ and $\psi = -40°$.

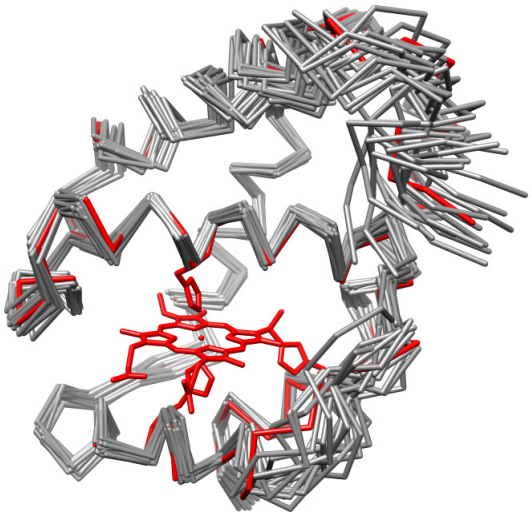

Figure S18: The structure refined with the pseudocontact shifts is shown in red among the 2KSC family. It is comprised within it, which indicates similar sampling of the conformational space with XPLOR. The regions of largest deviations between the refined model and the 2KSC average are those that display the largest ensemble rmsds without refinement (Figure 1a). We conclude that the measured pseudocontact shifts can be accommodated by the current family and that the backbone structures of the reduced and oxidized *Synechococcus* WT GlbN-A are, on average, similar.

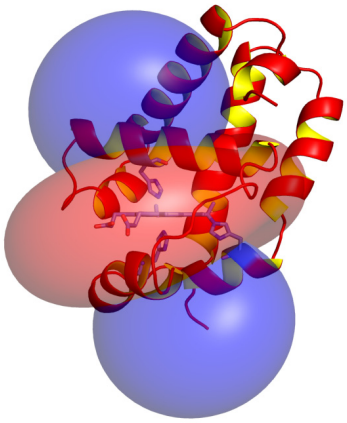

Figure S19: Pseudocontact shift map for *Synechococcus* WT GlbN-A in the ferric bishistidine state. Representation with Pymol (Delano Scientific) of the Numbat output [10]. The orientation of the structure is similar to that in Figure 1a of the text, with proximal His below the heme. The isoshift surfaces are drawn at +0.13 ppm (blue) and –0.13 ppm (red).

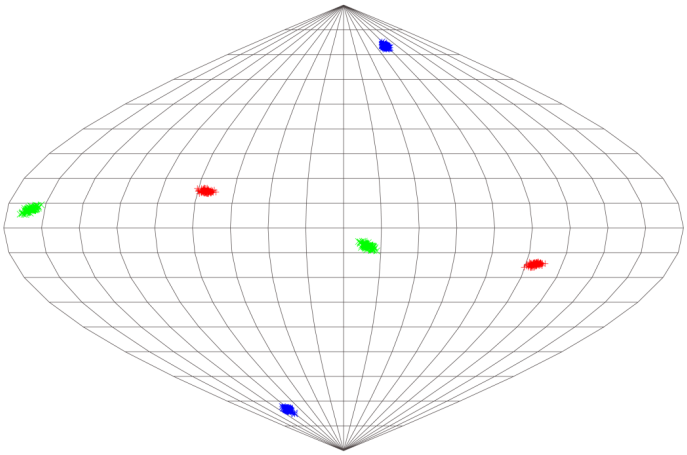

Figure S20: Sanson-Flamsteed equivalent projection of the magnetic susceptibility tensor for *Synechococcus* WT GlbN-A in the ferric bishistidine state. The z axis (vertical) is normal to the heme plane. The figure illustrates the tilt and the well-defined orientation of the tensor. Generated with Numbat [10].

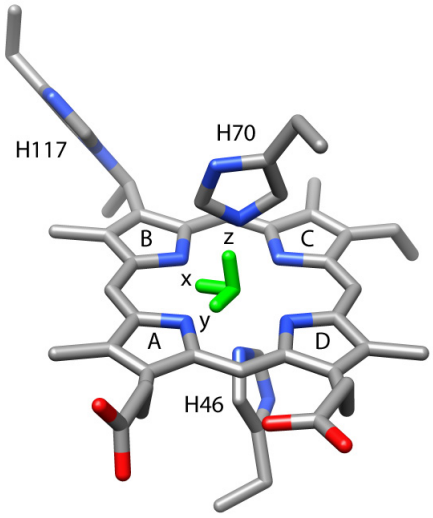

Figure S21: Magnetic susceptibility tensor of *Synechococcus* WT Fe(III)GlbN-A after refinement of 2KSC model 2. The tensor axes are represented as green sticks. The z direction lies practically in the plane normal to the heme passing through the nitrogens of pyrrole B and D.